

Plasmon-enhanced waveguide for dispersion compensation in mid-infrared quantum cascade laser frequency combs

YVES BIDAUX^{1*}, ILIA SERGACHEV², WOLF WUESTER¹, RICHARD MAULINI², TOBIAS GRESCH², ALFREDO BISMUTO², STÉPHANE BLASER², ANTOINE MULLER², AND JÉRÔME FAIST¹

¹Institute for Quantum Electronics, ETH-Zurich, CH-8093 Zurich, Switzerland

²Alpes Lasers SA, Avenue des Pâquiers 1, CH-2072 Saint-Blaise, Switzerland

*Corresponding author: bidauxy@phys.ethz.ch

Compiled March 1, 2017

We demonstrate dispersion compensation in mid-infrared quantum cascade laser frequency combs emitting at $7.8 \mu\text{m}$ using the coupling of a dielectric waveguide to a plasmonic resonance in the top cladding layer of the latter. Devices with group velocity dispersion as low as $-40 \text{ fs}^2/\text{mm}$ were fabricated and narrow beatnotes with a FWHM linewidth below 1 kHz were measured on the whole operation range. The optical output power reaches 275 mW and the optical spectrum spans 60 cm^{-1} . The multi-heterodyne beating spectrum of two devices was measured and spans 46 cm^{-1} , demonstrating the potential of dispersion engineered waveguides for the fabrication of highly stable and reliable quantum cascade laser frequency combs with high output power across the mid-infrared. © 2017 Optical Society of America

OCIS codes: (140.0140) Lasers and laser optics; (140.3070) Infrared and far-infrared lasers; (140.5965) Semiconductor lasers, quantum cascade

<http://dx.doi.org/10.1364/ao.XX.XXXXXX>

Quantum cascade lasers [1] (QCLs) are wavelength-agile semiconductor devices. Unlike quantum-well semiconductor lasers, QCLs have the flexibility to operate at any wavelength within a broad spectral range in the mid- to far-infrared. After years of active development, multi-watt level output powers at room temperature [2–4] as well as high efficiency [5, 6], low consumption [7] and broad tuning ranges [8, 9] are available across the whole mid-IR. Because of these unique features QCLs have become one of the most used light sources in the mid-infrared. Recently, it has been demonstrated that QCLs can operate as frequency combs (FCs) both in mid-infrared [10, 11] and THz frequencies [12, 13] and their usability in dual-comb spectroscopy setups has been demonstrated [14, 15]. These hold the promise of high resolution and high sensitivity spectrometers with no moving parts. Thanks to the cascading scheme of the QCL multiple active region can be heterogeneously stacked in a single waveguide and yield ultra-broadband lasers. The gain of QCLs can therefore reach 10% of the central wavelength. However, FC operation of QCLs is typically limited to a small portion of the dynamic range of the laser. For large optical spectrum spans the combs have the tendency to be destabilized and to enter the so called high phase noise regime [16]. Nevertheless, it was recently shown that the performances of QCL FCs can be improved by compensating their dispersion using Gires Tournois

effect. Multi-layer dielectric coatings (GTI) were deposited directly on the lasers back facets [16]. The coated devices featured a low group velocity dispersion (GVD) and frequency comb operation was observed on the complete dynamic range. However, the fabrication of high quality GTI coatings is challenging since due to the optical absorption of the materials used they overheat and burn. These are therefore incompatible with high optical output power and alternative solutions are required.

In this work we investigate how the dispersion of QCLs can be controlled by waveguide engineering. Similar work has been done in the past in the field of optical fibers in order to obtain zero dispersion fibers for telecommunication applications. For example, designing an optical fiber based on a triple clad index profile allowed to take advantage of the coupling of the core and ring modes of the fiber in order to achieve wideband dispersion slope compensation [17]. At $7.8 \mu\text{m}$ the GVD of InP is positive [18] the waveguide GVD should therefore be made negative in order to compensate for the material dispersion. However, a standard narrow ridge waveguide naturally has a positive GVD due to the increasing leakage of the optical mode into the waveguide sidewalls for longer wavelengths [19]. In this work we use a plasmon-enhanced waveguide. In such a waveguide the active region is placed between two low doped InP bottom and top claddings. In the last layer of the top cladding the

doping is increased in order to shift the plasma frequency close to the laser frequency. The high decrease of the refractive index in this layer has the effect to increase the confinement of the fundamental mode and decrease optical losses associated with the metallic top contact of the device [20]. The design of the waveguide used is detailed in Table 1.

Material	Thickness	Doping	Refractive index
Au	0.3 μm		50
InP	0.4 μm	1e19 cm^{-3}	1.3
InP	0.5 μm	5e18 cm^{-3}	2.4
InP	0.4 μm	1e17 cm^{-3}	3.08
InP	2.0 μm	2e16 cm^{-3}	3.09
InGaAs	0.25 μm	3e16 cm^{-3}	3.44
Active region	2.3 μm		3.35
InGaAs	0.2 μm	3e16 cm^{-3}	3.44
InP	2.5 μm	2e16 cm^{-3}	3.09
InP Substrate		4e18 cm^{-3}	2.54

Table 1. Schematic vertical cross section of laser structure waveguide. The refractive indices are computed at the laser central frequency: 1250 cm^{-1} .

The profile of the fundamental mode (at the lasing frequency: 1250 cm^{-1} , blue curve) was computed and is shown in 1D along the vertical axis in Fig. 1 (a) and in 2D in Fig. 1 (c). Because of the addition of a highly doped InP layer, the waveguide can also guide a surface plasmon mode. The profile of the plasmon mode (at the frequency: 700 cm^{-1} , red curve) was also computed and is shown in 1D along the vertical axis in Fig. 1 (a) and in 2D in Fig. 1 (b).

In order to study how the coupling of these two optical modes influences their dispersion, their effective refractive indices were computed as a function of the optical frequency for various top cladding thickness ($T = 1.0$ to $3.0 \mu\text{m}$). The dispersion of both modes is shown in Fig. 1 (d). The GVD of the fundamental mode was computed for each step and is shown in Fig. 1 (e). The coupling of the fundamental mode to the plasmon mode is proportional to the overlap factor between the fundamental mode and the highly doped InP layer (red area). This reflects on the dispersion. When the top cladding thickness is reduced, the coupling of the modes is increased and the GVD of the fundamental mode is reduced. This is shown in Fig. 1 (f), demonstrating that the coupling to the plasmon mode allows to tune the dispersion of the fundamental mode of the waveguide.

A QCL with an active region based on a single stack double-phonons QCL design emitting at $7.8 \mu\text{m}$ was grown. The band structure of the device is reported in [21]. The device was processed to a $10.5 \mu\text{m}$ wide Fabry-Perot ridge buried in InP [22] and cleaved to a 3 mm long bar. The waveguide design is detailed in Table 1. The device was soldered epi-up on a copper submount. The gain and the dispersion of the device were measured using the so called Fourier-Transform technique [23] and the deduced net modal gain and spectrally resolved GVD at $-20 \text{ }^\circ\text{C}$ for a current of 275 mA are shown in Fig. 2 (a) and (b). The waveguide dispersion was computed taking into account the

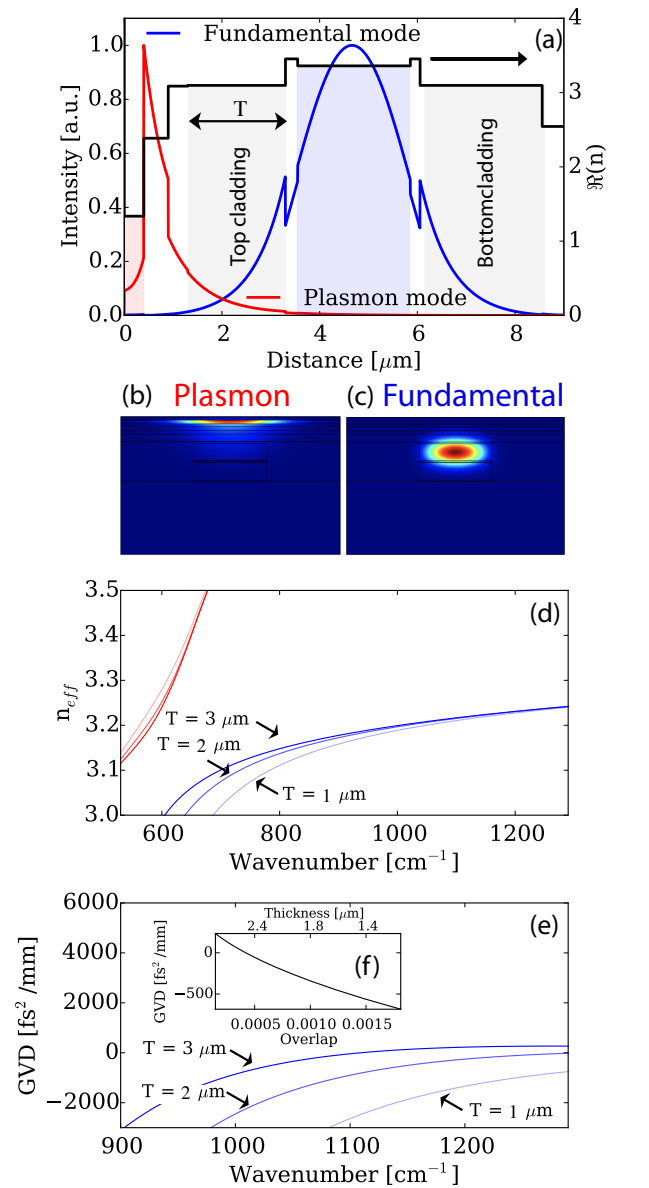


Fig. 1. (a) Refractive index profile along the growth axis (Black curve) and 1D computed waveguide fundamental mode at 1250 cm^{-1} (Blue curve) and plasmon mode at 700 cm^{-1} (Red curve). The red area indicates the highly doped InP layer, the black area indicates the top cladding layer and the blue area indicates the active region. (b) and (c) 2D profile of the plasmon and fundamental mode. (d) Effective refractive index of both the plasmon and fundamental modes as a function of the optical frequency for a top cladding thickness varying from 1.0 (shaded red and blue) to $3.0 \mu\text{m}$. (e) GVD of the fundamental mode. (f) GVD of the fundamental mode as a function of the overlap between the fundamental mode and the plasmonic layer at the lasing frequency (1250 cm^{-1}).

materials dispersion [18] while the gain induced dispersion was computed using Kramers-Kronig relation from the experimental gain curve. The total GVD is displayed on Fig. 2 (b) and shows a good agreement with the measured value). At 1250 cm^{-1} the measured GVD is $-40 \pm 150 \text{ fs}^2/\text{mm}$ confirming the low dispersion of the fabricated device. The uncertainty was deduced

comparing three subsequent measurements.

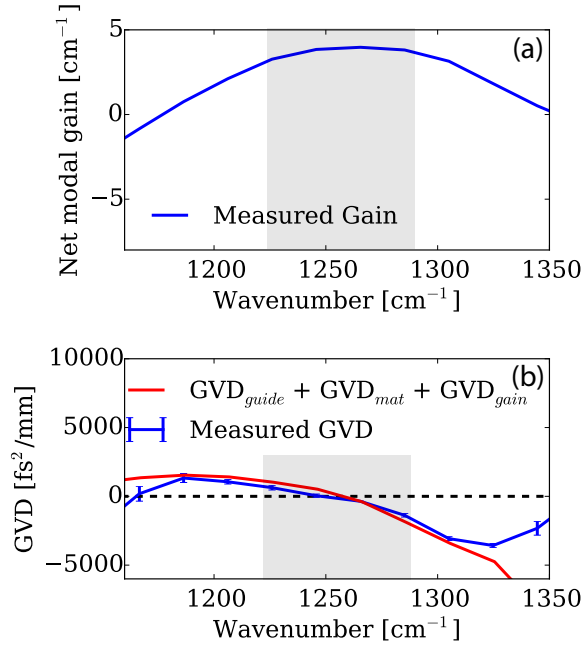


Fig. 2. Measured gain (a) and GVD (b). The gain induced dispersion was computed using Kramers-Kronig relation from the gain curve and added to the computed waveguide dispersion (red curve). At 1250 cm^{-1} the measured GVD is $-40 \text{ fs}^2/\text{mm}$ (blue curve). The shaded area indicates the measured frequency span of the FC.

The output power of the device was then measured as a function of current for heatsink temperatures ranging from -20°C to 50°C . It reached up to 275 mW at -20°C as shown in Fig. 3 (a). Comb operation was characterized. The beatnote frequency was measured with a resolution bandwidth (RBW) of 200 Hz varying the heat-sink temperature from -20°C to 10°C for various currents and is displayed in Fig. 3 (b). The beat frequency tunes with temperature ($1.5 \cdot 10^{-3} \text{ GHz/K}$) and current ($9.7 \cdot 10^{-2} \text{ GHz/A}$) as shown in Fig. 3 (b). This corresponds to a tuning rate of the group index of $\frac{1}{n_g} \frac{dn_g}{dT} = 10^{-4} \text{ K}^{-1}$ which is higher than the tuning rate of the effective index in QCLs $\frac{1}{n_{eff}} \frac{dn_{eff}}{dT} = 8 \cdot 10^{-5} \text{ K}^{-1}$ [22]. This allows to approximate the tuning rate of the carrier envelope frequency of the QCL FCs to 0.8 GHz/K.

The optical spectrum of the device was measured using a FTIR. At -20°C and for a current of 750 mA an optical frequency span of up to 60 cm^{-1} was measured. The spectrum is displayed in Fig. 4 (a). The corresponding RF spectrum was measured with a RBW of 200 Hz. The spectrum displayed in Fig. 4 (b) shows a FWHM of 690 Hz which suggests comb operation of the QCL.

In order to demonstrate the capabilities of the fabricated devices for dual-comb spectroscopy, the multi-heterodyne beating spectrum [15] of two of the devices was measured. The heatsink temperature was set to -15°C and the lasers current optimized in order to maximize the span of the multi-heterodyne beating spectrum. The first laser (FC_1) current was set to 782 mA and the second laser (FC_2) current to 697 mA. The mixed optical beam was focused on a MCT detector, recorded using an oscillo-

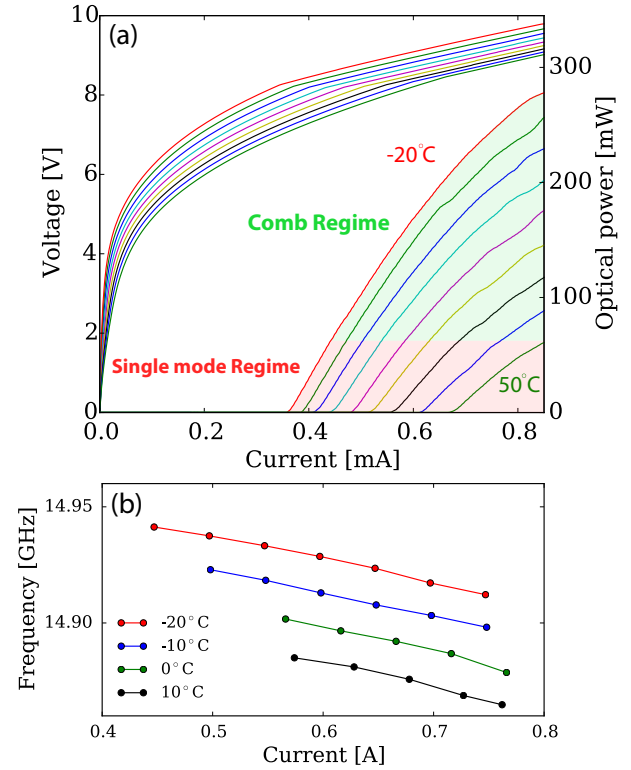


Fig. 3. (a) Current-voltage-light characteristics of the laser in CW for different submount temperatures. (b) Recorded beatnote frequency as a function of operating current and submount temperatures. The beat frequency is tuning with temperature ($1.5 \cdot 10^{-3} \text{ GHz/K}$) and current ($9.7 \cdot 10^{-2} \text{ GHz/A}$), corresponding to a tuning rate of the group index of $\frac{1}{n_g} \frac{dn_g}{dT} = 10^{-4} \text{ K}^{-1}$.

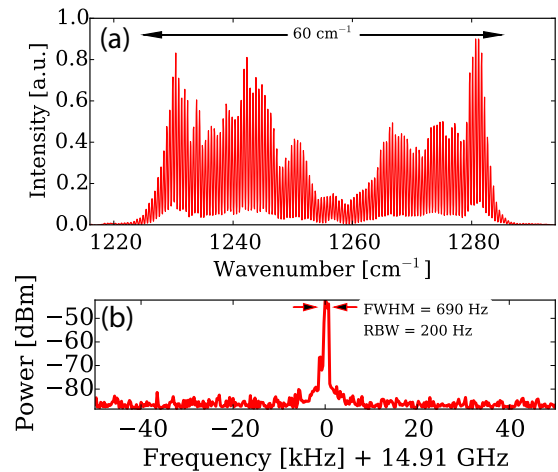


Fig. 4. (a) Optical spectrum measured for a current of 750 mA at a heatsink temperature of -20°C . An optical frequency span of up to 60 cm^{-1} is measured. (b) Corresponding RF spectrum. A beatnote with a FWHM of 690 Hz is measured with a RBW of 200 Hz.

scope and Fourier transformed at a repetition rate of 10 kHz. 93 modes are observed on the multi-heterodyne beating spectrum

displayed in Fig. 5 (b). As the comb free spectral range is approximately 0.49 cm^{-1} , this corresponds to an optical bandwidth of 46 cm^{-1} . The FWHM of one line is 400 kHz , which corresponds to a temperature or current drift of approximately $\delta T = 0.26 \text{ K}$ or $\delta I = 4 \text{ mA}$ respectively.

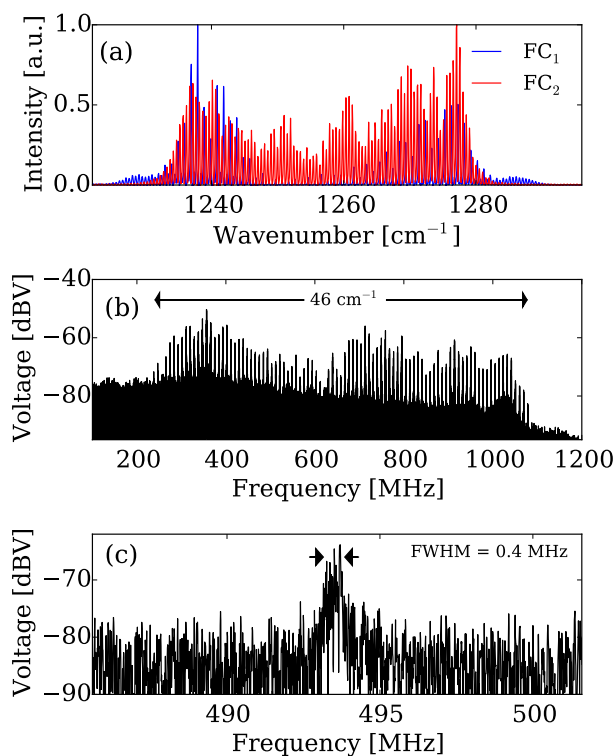


Fig. 5. (a) Optical spectrum of FC₁ for a current of 800 mA and FC₂ for a current of 700 mA. (b) and (c) The multi-heterodyne beating spectrum of the two FCs measured spans 46 cm^{-1} and has a FWHM of 400 kHz .

To conclude, by taking advantage of the dispersion of plasmon resonances we were able to engineer the dispersion of mid-infrared QCL FCs. The fabricated devices have a very low GVD and no high phase noise regime was observed. This leads to comb operation in significantly wider range of currents and temperatures. In particular, an output power of 275 mW was obtained for an optical frequency span of up to 60 cm^{-1} at $7.8 \mu\text{m}$. Finally, the capability of the devices for dual comb spectroscopy was demonstrated by measuring the multi-heterodyne beating spectrum of two devices which covers a span of 46 cm^{-1} .

FUNDING INFORMATION

Swiss National Science (SNSF); DARPA program SCOUT.

REFERENCES

1. J. Faist, F. Capasso, D. L. Sivco, C. Sirtori, A. L. Hutchinson, and A. Y. Cho, *Science* **264**, 553 (1994).
2. Y. Bai, N. Bandyopadhyay, S. Tsao, S. Slivken, and M. Razeghi, *Applied Physics Letters* **98**, 181102 (2011).
3. I. Sergachev, R. Maulini, A. Bismuto, S. Blaser, T. Gresch, and A. Muller, *Optics Express* **24**, 19063 (2016).
4. A. Bismuto, Y. Bidaux, S. Blaser, R. Terazzi, T. Gresch, M. Rochat, A. Muller, C. Bonzon, and J. Faist, *Optics Express* **24**, 10694 (2016).

5. Q. Y. Lu, Y. Bai, N. Bandyopadhyay, S. Slivken, and M. Razeghi, *Applied Physics Letters* **98**, 181106 (2011).
6. R. Maulini, A. Lyakh, A. Tsekoun, R. Go, C. Pflügl, L. Diehl, F. Capasso, and C. K. N. Patel, *Applied Physics Letters* **95**, 151112 (2009).
7. A. Bismuto, S. Blaser, R. Terazzi, T. Gresch, and A. Muller, *Optics Express* **23**, 5477 (2015).
8. Y. Bidaux, A. Bismuto, C. Tardy, R. Terazzi, T. Gresch, S. Blaser, A. Muller, and J. Faist, *Applied Physics Letters* **107**, 221108 (2015).
9. B. G. Lee, M. A. Belkin, R. Audet, J. MacArthur, L. Diehl, C. Pflügl, F. Capasso, D. C. Oakley, D. Chapman, A. Napoleone, D. Bour, S. Corzine, G. Höfler, and J. Faist, *Applied Physics Letters* **91**, 231101 (2007).
10. A. Hugi, G. Villares, S. Blaser, H. C. Liu, and J. Faist, *Nature* **492**, 229 (2012).
11. Q. Y. Lu, M. Razeghi, S. Slivken, N. Bandyopadhyay, Y. Bai, W. J. Zhou, M. Chen, D. Heydari, A. Haddadi, R. McClintock, M. Amanti, and C. Sirtori, *Applied Physics Letters* **106**, 051105 (2015).
12. M. Rösch, G. Scalari, M. Beck, and J. Faist, *Nature Photonics* (2014).
13. D. Burghoff, T.-Y. Kao, N. Han, C. W. I. Chan, X. Cai, Y. Yang, D. J. Hayton, J.-R. Gao, J. L. Reno, and Q. Hu, *Nature Photonics* **8**, 462 (2014).
14. M. Rösch, G. Scalari, G. Villares, L. Bosco, M. Beck, and J. Faist, *Applied Physics Letters* **108**, 171104 (2016).
15. G. Villares, A. Hugi, S. Blaser, and J. Faist, *Nature Communications* **5**, 5192 (2014).
16. G. Villares, S. Riedi, J. Wolf, D. Kazakov, M. J. Süess, P. Jouy, M. Beck, and J. Faist, *Optica* **3**, 252 (2016).
17. V. M. Schneider and J. West, *Electronics Letters* **38**, 306 (2002).
18. E. D. Palik and G. Ghosh, eds., *Handbook of optical constants of solids* (Academic Press, San Diego, 1998).
19. J. Faist, G. Villares, G. Scalari, M. Rösch, C. Bonzon, A. Hugi, and M. Beck, *Nanophotonics* **5** (2016).
20. C. Sirtori, J. Faist, F. Capasso, D. L. Sivco, A. L. Hutchinson, and A. Y. Cho, *Applied Physics Letters* **66**, 3242 (1995).
21. Y. Bidaux, R. Terazzi, A. Bismuto, T. Gresch, S. Blaser, A. Muller, and J. Faist, *Journal of Applied Physics* **118**, 093101 (2015).
22. A. Bismuto, Y. Bidaux, C. Tardy, R. Terazzi, T. Gresch, J. Wolf, S. Blaser, A. Muller, and J. Faist, *Optics Express* **23**, 29715 (2015).
23. D. Hofstetter and J. Faist, *IEEE Photonics Technology Letters* **11**, 1372 (1999).

REFERENCES

1. J. Faist, F. Capasso, D. L. Sivco, C. Sirtori, A. L. Hutchinson, and A. Y. Cho, "Quantum Cascade Laser," *Science* **264**, 553–556 (1994).
2. Y. Bai, N. Bandyopadhyay, S. Tsao, S. Slivken, and M. Razeghi, "Room temperature quantum cascade lasers with 27% wall plug efficiency," *Applied Physics Letters* **98**, 181102 (2011).
3. I. Sergachev, R. Maulini, A. Bismuto, S. Blaser, T. Gresch, and A. Muller, "Gain-guided broad area quantum cascade lasers emitting 235 W peak power at room temperature," *Optics Express* **24**, 19063 (2016).
4. A. Bismuto, Y. Bidaux, S. Blaser, R. Terazzi, T. Gresch, M. Rochat, A. Muller, C. Bonzon, and J. Faist, "High power and single mode quantum cascade lasers," *Optics Express* **24**, 10694 (2016).
5. Q. Y. Lu, Y. Bai, N. Bandyopadhyay, S. Slivken, and M. Razeghi, "2.4 W room temperature continuous wave operation of distributed feedback quantum cascade lasers," *Applied Physics Letters* **98**, 181106 (2011).
6. R. Maulini, A. Lyakh, A. Tsekoun, R. Go, C. Pflügl, L. Diehl, F. Capasso, and C. K. N. Patel, "High power thermoelectrically cooled and uncooled quantum cascade lasers with optimized reflectivity facet coatings," *Applied Physics Letters* **95**, 151112 (2009).
7. A. Bismuto, S. Blaser, R. Terazzi, T. Gresch, and A. Muller, "High performance, low dissipation quantum cascade lasers across the mid-IR range," *Optics Express* **23**, 5477 (2015).
8. Y. Bidaux, A. Bismuto, C. Tardy, R. Terazzi, T. Gresch, S. Blaser, A. Muller, and J. Faist, "Extended and quasi-continuous tuning of quantum cascade lasers using superstructure gratings and integrated heaters," *Applied Physics Letters* **107**, 221108 (2015).
9. B. G. Lee, M. A. Belkin, R. Audet, J. MacArthur, L. Diehl, C. Pflügl, F. Capasso, D. C. Oakley, D. Chapman, A. Napoleone, D. Bour, S. Corzine, G. Höfler, and J. Faist, "Widely tunable single-mode quantum cascade laser source for mid-infrared spectroscopy," *Applied Physics Letters* **91**, 231101 (2007).
10. A. Hugi, G. Villares, S. Blaser, H. C. Liu, and J. Faist, "Mid-infrared frequency comb based on a quantum cascade laser," *Nature* **492**, 229–233 (2012).
11. Q. Y. Lu, M. Razeghi, S. Slivken, N. Bandyopadhyay, Y. Bai, W. J. Zhou, M. Chen, D. Heydari, A. Haddadi, R. McClintock, M. Amanti, and C. Sirtori, "High power frequency comb based on mid-infrared quantum cascade laser at $\lambda \sim 9 \mu\text{m}$," *Applied Physics Letters* **106**, 051105 (2015).
12. M. Rösch, G. Scalari, M. Beck, and J. Faist, "Octave-spanning semiconductor laser," *Nature Photonics* (2014).
13. D. Burghoff, T.-Y. Kao, N. Han, C. W. I. Chan, X. Cai, Y. Yang, D. J. Hayton, J.-R. Gao, J. L. Reno, and Q. Hu, "Terahertz laser frequency combs," *Nature Photonics* **8**, 462–467 (2014).
14. M. Rösch, G. Scalari, G. Villares, L. Bosco, M. Beck, and J. Faist, "On-chip, self-detected terahertz dual-comb source," *Applied Physics Letters* **108**, 171104 (2016).
15. G. Villares, A. Hugi, S. Blaser, and J. Faist, "Dual-comb spectroscopy based on quantum-cascade-laser frequency combs," *Nature Communications* **5**, 5192 (2014).
16. G. Villares, S. Riedi, J. Wolf, D. Kazakov, M. J. Süess, P. Jouy, M. Beck, and J. Faist, "Dispersion engineering of quantum cascade laser frequency combs," *Optica* **3**, 252 (2016).
17. V. M. Schneider and J. West, "Analysis of wideband dispersion slope compensating optical fibres by supermode theory," *Electronics Letters* **38**, 306–307 (2002).
18. E. D. Palik and G. Ghosh, eds., *Handbook of optical constants of solids* (Academic Press, San Diego, 1998).
19. J. Faist, G. Villares, G. Scalari, M. Rösch, C. Bonzon, A. Hugi, and M. Beck, "Quantum Cascade Laser Frequency Combs," *Nanophotonics* **5** (2016).
20. C. Sirtori, J. Faist, F. Capasso, D. L. Sivco, A. L. Hutchinson, and A. Y. Cho, "Quantum cascade laser with plasmon-enhanced waveguide operating at 8.4 μm wavelength," *Applied Physics Letters* **66**, 3242 (1995).
21. Y. Bidaux, R. Terazzi, A. Bismuto, T. Gresch, S. Blaser, A. Muller, and J. Faist, "Measurements and simulations of the optical gain and anti-reflection coating modal reflectivity in quantum cascade lasers with multiple active region stacks," *Journal of Applied Physics* **118**, 093101 (2015).
22. A. Bismuto, Y. Bidaux, C. Tardy, R. Terazzi, T. Gresch, J. Wolf, S. Blaser, A. Muller, and J. Faist, "Extended tuning of mid-ir quantum cascade lasers using integrated resistive heaters," *Optics Express* **23**, 29715 (2015).
23. D. Hofstetter and J. Faist, "Measurement of semiconductor laser gain and dispersion curves utilizing Fourier transforms of the emission spectra," *IEEE Photonics Technology Letters* **11**, 1372–1374 (1999).